Kinetic Sensitivity of a Receptor-Binding Radiopharmaceutical: Technetium-99m Galactosyl-Neoglycoalbumin

David R. Vera, E. Steve Woodle, and Robert C. Stadalnik

Division of Nuclear Medicine, Department of Radiology; and Department of Surgery; University of California, Davis, Medical Center

Kinetic sensitivity is the ability of a physiochemical parameter to alter the time-activity curve of a radiotracer. The kinetic sensitivity of liver and blood time-activity data resulting from a single bolus injection of [^{99m}Tc]galactosyl-neoglycoalbumin ([Tc]NGA) into healthy pigs was examined. Three parameters, hepatic plasma flow scaled as flow per plasma volume, ligand-receptor affinity, and total receptor concentration, were tested using [Tc]NGA injections of various molar doses and affinities. Simultaneous measurements of plasma volume (iodine-125 human serum albumin dilution), and hepatic plasma flow (indocyanine green extraction) were performed during 12 [Tc]NGA studies. Paired data sets demonstrated differences ($P(\chi^2) < 0.01$) in liver and blood time-activity curves in response to changes in each of the tested parameters. We conclude that the [Tc]NGA radiopharmacokinetic system is therefore sensitive to hepatic plasma flow, ligand-receptor affinity, and receptor concentration. In vivo demonstration of kinetic sensitivity permits delineation of the physiologic parameters that determine the biodistribution of a radiopharmaceutical. This delineation is a prerequisite to a valid analytic assessment of receptor biochemistry via kinetic modeling.

J Nucl Med 30:1519–1530, 1989

Receptor-binding radiopharmaceuticals exist for brain (*1–5*), heart (*6*), and liver (*7*) tissue. The ultimate purpose of these agents is the in vivo measurement of receptor biochemistry (*8–10*). To achieve this goal a variety of techniques (*11–17*) have been developed which attempt to measure receptor concentration and/or ligand receptor affinity. Although demonstrations of altered imaging data in response to pathophysiology have been reported (*7,12,18–21*), within each of these studies there exists no evidence to rule out the possibility that such changes were influenced by alterations in other parameters such as tissue plasma flow or extravascular permeability. Consequently, the kinetic analysis of these data may be assigning values to the wrong physiologic parameters.

The in vivo assay of receptor biochemistry via analysis of time-activity data is based on the assumption of kinetic sensitivity. When this concept is applied to nuclear medicine, kinetic sensitivity can be defined as the ability of a physiochemical parameter to alter the time-activity data of a radioindicator. For example, if the kinetic data is sensitive to receptor concentration, injection of [^{99m}Tc]galactosyl-neoglycoalbumin ([Tc]NGA) into patients with different receptor concentrations (but similar distribution volumes and plasma flow) will result in liver time-activity curves with different shapes. Conversely, if [Tc]NGA time-activity data is not sensitive to receptor concentration each study would produce superimposable kinetic data; such a condition would render the inference of receptor concentration impossible.

This paper presents in vivo evidence of kinetic sensitivity to hepatic plasma flow, [Tc]NGA affinity, and receptor concentration for the [Tc]NGA pharmacokinetic system.

MATERIALS AND METHODS

Experimental Design

Our experimental design consisted of seven steps. First, select the physiochemical parameters to be tested. Selection was based on the [Tc]NGA kinetic model (Fig. 1) (*13*) which

Received Nov. 23, 1988; revision accepted Apr. 18, 1989.

For reprints contact: Robert C. Stadalnik, MD, Div. of Nuclear Medicine, University of California, Davis, Medical Center, 2315 Stockton Blvd., Sacramento, CA 95817.

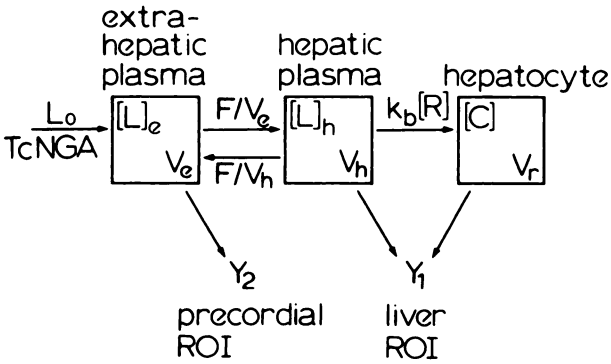

FIGURE 1
The kinetic model for [Tc]NGA uptake is composed of two processes: a hemodynamic phase controlled by hepatic plasma flow, and systemic and hepatic plasma volumes; and a receptor-binding phase controlled by the forward-binding rate constant and receptor concentration. See Table 1 for a list of symbols.

predicted that hepatic and blood time-activity data, Y_1 and Y_2, are controlled by the following physiologic parameters: (a) scaled hepatic plasma flow, F/V_e; (b) ligand receptor affinity, or more specifically, the forward binding rate constant, k_b; and (c) receptor concentration, [R]. Symbols are listed in Table 1. Second, pose three hypotheses: (I) liver and plasma time-activity data is independent of scaled hepatic plasma flow; (II) liver and plasma time-activity data is independent of ligand carbohydrate density; and (III) liver and blood time-activity data is independent of scaled molar dose, the moles of [Tc]NGA injected per liter of plasma volume per kilogram of liver weight. Rejection of each hypothesis would then support the existence of kinetic sensitivity to the corresponding parameter. Third, select, if possible, independent variables which control each parameter. In this study, NGA galactose density and NGA molar dose were used to directly control NGA affinity and sensitivity to receptor concentration, respectively. Fourth, perform controlled [Tc]NGA experiments. Controls and independent measurements were implemented during 12 [Tc]NGA studies. Fifth, arrange studies into pairs; then place them into comparable groups. Sixth, inspect each study-pair for consistency with the kinetic model. For example, when comparing two sets of time-activity data, the liver curve resulting from a lower molar dose, higher galactose density (ligand-receptor affinity), and higher scaled plasma flow should rise faster and peak earlier. Seventh, perform a statistical test for independence (χ^2) of the time-activity data within study pairs. Reject each hypothesis if all study pairs within each comparable group are consistent with the kinetic model and exhibit statistical independence, defined as $P(\chi^2) < 0.01$.

Indicator Preparation

Technetium-99m NGA functional imaging, steady-state indocyanine green extraction measurements (*22*), and plasma volume measurements were performed using 12 adolescent pigs (14–21 kg). Galactosyl-neoglycoalbumin was synthesized as previously described (*23*). Two different carbohydrate densities, 27 and 37 galactose residues per albumin, were used. In vitro binding measurements [^{125}I]NGA (chloramine-T) to rabbit liver membrane (*24*) indicated that the forward-binding rate constant and equilibrium constant of a [^{125}I]NGA with 37 galactose groups per albumin molecule were twice that of [^{125}I]NGA with a galactose density of 25. Electrolytic reduction was employed for technetium labeling of NGA (*23*) prior to each pig study. Quality control of each [Tc]NGA preparation consisted if size-exclusion high performance liquid chromatography (HPLC) (*23*) and required that >95% of the activity existed as labeled monomeric NGA. Iodine-125 human serum albumin ([^{125}I]HSA) (Mallinckrodt, St. Louis, MO) was column-purified (Sephadex, G-200). Indocyanine green (Hynson, Westcott & Dunning, Cardiogreen, Baltimore, MD) (ICG) was reconstituted with distilled water to a concentration of 12 mg/ml. Standards for ICG assay were prepared using autologous serum. Optical density measurements were conducted at 805 nm with autologous serum in the reference cell. Counting standards were prepared for each tracer. Assay for radioactivity was carried out in a gamma well counter using energy windows of 100–200 keV for ^{99m}Tc, and 15–40 keV for ^{125}I. Determination of ^{125}I activity was performed at least four days after the imaging study. All standards and samples were counted in polypropylene test tubes filled to a consistent volume.

Animal Studies

A single study consisted of the following sequence: (a) installation of catheters, (b) withdrawal of autologous blood, (c) ICG bolus/infusion, (d) injection of [^{125}I]HSA, (e) injection of [Tc]NGA, and (f) dynamic planar imaging. Anesthesia was induced with 5% halothane and, after placement of an endotracheal tube, maintained with 0.3–0.5% halothane and 60% nitrous oxide (2 l/min) and oxygen (1–2 l/min). Rectal temperature was maintained at 39°C with a thermostatically-controlled heating blanket. Arterial and a double lumen central venous catheters were placed in the internal carotid artery and internal jugular vein, respectively. Mean arterial pressure was monitored and maintained within 90–110 mmHg by adjustment of the halothane flow. A hepatic vein catheter (7 French) was guided to the wedge position of the left medial lobe with the aid of an 0.036-gauge wire which was previously introduced via the external jugular vein and advanced to the suprahepatic vena cava. This placement required a midline laparotomy and division of the anterior and posterior peritoneal attachments of the liver. Placement of the catheter into the hepatic vein was directed by visual inspection. Patency of the hepatic vein catheter was maintained by a slow infusion (≈5 drop/min) of heparinized saline (1000 units/l). Hematocrit was assayed every 15 min; stable values were required prior to [Tc]NGA injection. After obtaining serum for ICG standards, a constant intravenous infusion of ICG (0.015 mg/kg/min) was initiated with a bolus of the indicator (0.4 mg/kg) via the central venous catheter. After 20 min of infusion, arterial blood samples were obtained at 10-min intervals for verification of ICG steady state, which was defined as <5% change in serum ICG concentration over a 30-min period (*22*). Following pretreatment with HSA, the second port of the central venous catheter was used to introduce 20μCi of [^{125}I]HSA. Arterial samples for assay of plasma radioactivity were drawn at 15 and 30 min after injection. Sampling for [^{125}I]HSA was continued at 30-min intervals up to 2 hr postinjection. After verification of ICG steady state and stable hematocrit, the animal was placed under a scintillation camera

TABLE 1
Symbols

Symbols	Description	Units	Eq	Symbols	Description	Units	Eq
C_k	Test criterion for model consistency of the kth controlling parameter		6	r	Rate of ICG infusion	mg min^{-1}	1
[C]	Ligand-receptor complex concentration	*M*	I	[R]	Receptor concentration	*M*	I
$\tilde{f}_{24}$	Fraction of the injected [Tc]NGA dose per liter of plasma during the 24th frame	l^{-1}	2a	$\tilde{S}_{ik}$	Relative sensitivity of the ith observer to the kth parameter		11
F	Hepatic plasma flow	l min^{-1}	1	t_{70}	Time at which the liver time-activity curve equals 70% of injected dose	min	6
$\tilde{F}$	Scaled liver plasma flow: hepatic plasma flow per liter of plasma	min^{-1}	3a	V_e	Extra-hepatic plasma volume	L	3a
				V_h	Hepatic plasma volume	L	3b
				V_p	Plasma volume	L	3b
				Y_1	Liver ROI data	cts	2a
$[ICG]_a$	Arterial ICG concentration	mg/l	1	Y_2	Precordial ROI data	cts	
$[ICG]_v$	Hepatic venous ICG concentration	mg/l	1	$\tilde{Y}_{1j}$	Fraction-of-injected [Tc]NGA activity in liver during the jth frame		2b
k_b	Forward-binding rate constant	M^{-1} min^{-1}	I	$\tilde{Y}_{2j}$	Fraction-of-injected [Tc]NGA activity in plasma during the jth frame		2a
k_{-b}	Reverse-binding rate constant	min^{-1}	I				
K_A	Association constant	M^{-1}		Y′	Second member of a study pair		8
$[L]_e$	NGA concentration in extra-hepatic plasma	*M*		$\Delta\tilde{v}_k$	Relative difference between the kth independent variable within a study pair		6
$[L]_h$	NGA concentration in hepatic plasma	*M*					
L_0	Amount of NGA injected	μmol	4	ν	Degrees of freedom		
$\tilde{L}_0$	Scaled molar dose: NGA per liter of plasma per kg of liver	μM kg^{-1}	4	ρ_{gal}	Galactose density		5
				$\sigma(\tilde{y}_{ij})^2$	Variance of $\tilde{y}_{ij}$		8
m_l	Liver mass	kg	4	$\Sigma\Delta\tilde{v}$	Net fractional change in the independent variables within a study pair		7
m	Number of data points in χ^2 calculation		10				
n	Number of frames in time-activity data		2a				
p	Kinetic parameter		11	χ^2	Chi-square		8
$P(\chi^2_r)$	Probability of exceeding χ^2_r by chance			χ^2_r	Reduced chi-square		10

(Nuclear Chicago, Pho-Gamma HP, Des Plaines, IL). Three pairs of hepatic venous and arterial samples were then drawn for assay of hepatic ICG extraction.

The [Tc]NGA functional imaging study was performed by methods previously detailed (*25*). Briefly, after positioning the animal for a ventral view of the heart and liver, a bolus dose (2–5 mCi) of [Tc]NGA was administered through the central venous catheter. Digital images 128x128 were acquired (ADAC Laboratories, DPS-2200; Milpitas, CA) in byte mode at a rate of 8 frames per minute. Hepatic venous and arterial blood samples were drawn at 3, 5, 10, 20, and 30 min after injection. A portion of each arterial sample was immediately centrifuged in a heparin-coated microcentrifuge tube (Brinkmann Instruments, Westbury, NY) from which 0.1cc of plasma was removed for radioactivity assay. Thirty minutes after [Tc]NGA injection computer acquisition was halted and the hepatic vein catheter was removed after visual conformation of its position within the hepatic vein. Following removal of the i.v. catheter, the rate of ICG infusion was measured with the same catheter, syringe, and ICG solution used during the study. Using standard image processing software, a region of interest (ROI) was defined which encompassed the heart without including activity from the liver. Also defined was a region which encompassed the entire liver, yet excluded activity within the precordium. Based on the precordial and liver ROIs, time-activity curves were then generated from the sequential images. These data, represented by Y_2 and Y_1, were in units of counts per 7.5-sec frame. Peak activity in the precordial ROI was used to define the first frame of the time-activity curve. At the conclusion of the study the liver was removed, drained of large vessel blood, and weighed. A sample of hepatic tissue was removed and assayed for ^{125}I activity.

Calculations

Hepatic plasma flow, plasma volume, scaled time-activity data, and hepatic plasma volume were obtained in the following manner. Serum samples obtained during ICG steady state were assayed for ICG concentration (mg/l) at 805 nm. Cal-

culation of hepatic plasma flow, F, utilized the Fick principle (*26*):

$$F = \frac{r}{[ICG]_a - [ICG]_v}, \quad (1)$$

where $[ICG]_a$ and $[ICG]_v$ equal arterial and hepatic venous ICG concentrations in mg/l, and r equals the rate of ICG infusion in mg/min. The plasma sample obtained 3 min after [Tc]NGA injection was assayed for the fraction of injected ^{99m}Tc per liter of plasma, and was designated $\tilde{f}_{24}$; where the subscript denotes the 24th frame of the dynamic study. The plasma volume was equated to the inverse of the Y-intercept resulting from a semilogarithmic plot of the fraction of injected ^{125}I per liter of sampled plasma versus time (15, 30, 60, 90, and 120 min post I-HSA injection). Multiplication of $\tilde{f}_{24}$ by total plasma volume, V_p, yielded the percentage of injected [Tc]NGA in the plasma at 3 min. The remainder of the [Tc] NGA dose was assigned to the liver. This calculation was based on conservation of [Tc]NGA between the liver and plasma. This assumption was validated by previous biodistribution studies in rabbits (*23*) which showed that at early time points the [Tc]NGA dose was conserved between blood pool and liver. Liver and blood time-activity curves were then scaled to fraction of injected dose based on the value calculated at 3 min after injection,

$$\left.\begin{aligned} \tilde{Y}_{2j} &= Y_{2j}\tilde{f}_{24}V_p/y_{2,24} \quad (2a)\\ \tilde{Y}_{1j} &= 1 - \tilde{Y}_{2j} \quad (2b)\end{aligned}\right\} j = 1 \ldots n,$$

where the subscript j denotes the frame number of the dynamic study, n is the number of frames in the study; and $y_{2,24}$ equals the counts within the precordial ROI in frame 24. Hepatic plasma volume was measured by scaling the fraction of injected ^{125}I per gram of sampled liver to total organ weight. This measurement assumed that 100% of the ^{125}I in the liver resided within the hepatic plasma.

Definitions

Scaled liver plasma flow, $\tilde{F}$, was defined as

$$\tilde{F} \equiv F/V_e, \text{ and} \quad (3a)$$

$$V_e = V_p - V_h, \quad (3b)$$

where V_e equals the extrahepatic plasma volume, and V_p equals plasma volume as measured by [^{125}I]HSA. We also defined two variables which directly determine two model parameters. Scaled molar dose controls the number of occupied receptors during the course of the [Tc]NGA study and is

$$\tilde{L}_o \equiv L_o/V_p/m_l, \quad (4)$$

where L_o equals the amount of injected NGA and m_l is the hepatic mass. The second variable, galactose density, is the mean number of galactose molecules attached to a single molecule of human serum albumin:

$$\rho_{gal} \equiv \#\text{ of galactose molecules per HSA.} \quad (5)$$

This variable determines [Tc]NGA-receptor affinity.

Model Consistency and Study Groups

All study pairs were examined for consistency with the kinetic model in the following manner. Our kinetic model predicted that reductions in scaled hepatic plasma flow, or ligand–receptor affinity would produce slower hepatic uptake and blood clearance. The model also predicted that lower values for scaled molar dose would increase hepatic uptake and blood clearance. If the differences in the time-activity data could not be explained by at least one parameter, the kinetic behavior of the study pair was deemed inconsistent with the model.

Figure 2 illustrates model consistency between two [Tc]NGA studies. Study 7 has more rapid hepatic uptake and blood clearance than study 8, which has a lower scaled plasma flow and higher scaled molar dose than study 7. Both studies used [Tc]NGA preparations of similar galactose density. This pair would be qualitatively inconsistent with the model if the scaled hepatic plasma flow of study 7 was lower or the scaled molar dose was higher than study 8.

These relationships were used to define a semiquantitative criterion C_k for model consistency by the kth variable

$$C_k \equiv \text{sign}(\Delta t_{70})/\text{sign}(\Delta \tilde{v}_k), \quad (6)$$

where $\Delta\tilde{v}_k$ is the relative change in the kth variable ($v_1 = \tilde{F}$, $v_2 = \rho_{gal}$, $v_1 = \tilde{L}_o$); t_{70} is the time when the liver time-activity curve equaled 70% of the injected activity; Δt_{70} is the difference within a study pair; and sign(x) yielded 1 or −1 based on the sign of x, or 0 when x = 0. Values for t_{70} were calculated by incrementing j (starting at j = 1) until $\tilde{Y}_{1j} \geq 0.7$; t_{70} in minutes then equaled 0.15j.

Each of the comparable study pairs from Table 2 were placed into one of three groups based on criteria listed in the Appendix. Group I contained the study pairs testable for kinetic sensitivity to scaled hepatic plasma flow. Figure 3 illustrates a study pair that was consistent with the model but did not satisfy Group I (or II or III) criteria. As a result, this pair could not be used to test kinetic sensitivity of scaled hepatic plasma flow. Within this pair (studies 10 and 12) the

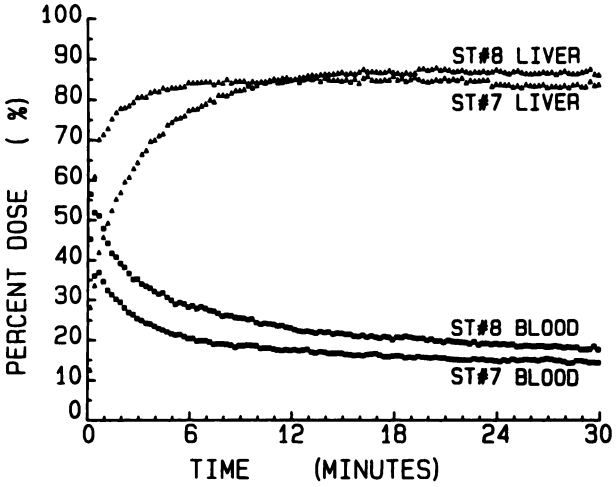

FIGURE 2
The relative kinetic behavior of studies 7 (only data-points from odd-valued frames are plotted) and 8 are consistent with the kinetic model. The decreased rate of hepatic uptake and blood clearance of study 8 (only data-points from odd-valued frames are plotted) is consistent with a lower scaled liver plasma flow and higher scaled molar dose (Table 4). Both studies used a [Tc]NGA preparation with the same galactose density.

TABLE 2
Physiochemical Measurements

Study no.	Experimental conditions: Galactose density (mole/mole)	Molar dose (nmol)	Liver weight (kg)	Plasma flow (l/min)	Hematocrit (%)	Plasma volume (l)	Hepatic plasma volume (l)
1	27	79.0	0.39	0.47	18	1.10	0.081
2	27	85.0	0.43	0.26	33	0.81	0.074
3	37	85.0	0.38	0.39	30	0.98	0.069
4	27	84.0	0.45	0.47	33	0.74	0.075
5	37	150.0	0.50	0.33	21	0.70	0.086
6	37	9.1	0.37	0.32	29	0.71	0.080
7	37	7.5	0.49	0.60	37	1.20	0.083
8	37	9.2	0.38	0.23	29	0.82	0.057
9	27	15.0	0.45	0.73	31	0.85	0.080
10	27	86.0	0.39	0.26	26	0.67	0.078
11	27	15.0	0.54	0.22	35	0.78	0.087
12	27	93.0	0.53	0.59	26	1.00	0.110

change in ρ_{gal} was within 10% as required by criterion *i* of Group I. However, sign($\Delta\tilde{v}_{\tilde{L}_o}$) did not equal sign($\Delta\tilde{v}_{\tilde{F}}$), and therefore, did not satisfy the second half of criterion *i*. According to the model, either a decrease in $\tilde{F}$ or an increase in $\tilde{L}_o$ could account for the differences observed in the time-activity curves of studies 10 and 12. Group II contained the study pairs testable for kinetic sensitivity to NGA-receptor affinity by eliminating pairs within which the study with the more rapid liver uptake used a higher carbohydrate density or lower scaled molar dose. Group III contained the study pairs testable for kinetic sensitivity to receptor concentration by eliminating study pairs within which the study with the faster liver uptake had the higher scaled liver plasma flow or used a higher carbohydrate density.

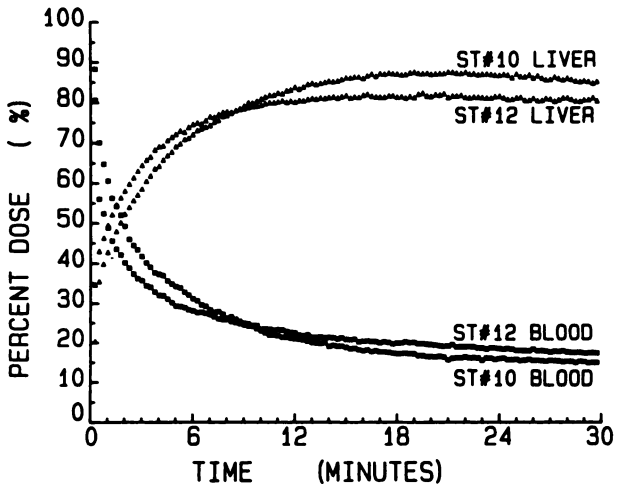

FIGURE 3
Comparison of studies 10 and 12 could not be used to test for kinetic sensitivity. The decreased rate in the hepatic uptake and blood clearance of study 10 (only data-points from odd-valued frames are plotted) was accompanied by a lower scaled plasma flow and a higher scaled molar dose. Although consistent with the model, either alteration (decrease in $\tilde{F}$, or increase in $\tilde{L}_o$) could account for the differences between the time-activity data of the study pair.

Semiquantitative Analysis

Lastly, we defined $\Sigma\Delta\tilde{v}$ as the net relative change in each variable, $\tilde{v}_{\tilde{F}}$, $\tilde{v}_{\rho_{gal}}$, and $\tilde{v}_{\tilde{L}_o}$, within a study pair

$$\Sigma\Delta\tilde{v} = \Sigma C_k \Delta\tilde{v}_k. \quad (7)$$

This index was used to test model consistency of all study pairs.

Statistical Methods

Study pairs deemed consistent (more specifically, not inconsistent) and testable were subjected to statistical analysis. Rejection of our three null hypotheses required a test for independence between Y and Y′. Thus, the χ^2 statistic was used to calculate the probability, $P(\chi^2)$, that the curves within each pair resulted from the same sample population. The following expression (*27*) was used:

$$\chi^2 = \sum_{j=24}^{n} \sum_{i}^{2} \frac{[\tilde{y}_{ij} - \tilde{y}'_{ij}]^2}{\sigma(\tilde{y}_{ij})^2}. \quad (8)$$

Variables $\tilde{Y}$ and $\tilde{Y}'$ represented the pair of scaled liver time-activity curves to be tested; thus, $\tilde{y}_{ij}$ equaled the fraction of injected dose within the jth frame of the ith ROI. The denominator of this equation, $\sigma(\tilde{y}_{ij})^2$, was the variance of $\tilde{y}_{ij}$, which was derived from the relative errors associated with: (a) y_{ij}, the counts within the jth frame of the ith ROI, (b) V_p, the plasma volume measurement, (c) $\tilde{f}_{24}$, the fraction of injected activity per liter of plasma within the 3-min blood sample, and (d) $y_{2,24}$, the counts within the precordial ROI at 3 min. Starting the chi-squared calculation at frame 24 eliminated the first 3 min of time-activity data from the analysis. This period is dominated by mixing of the radiopharmaceutical within the plasma volume. Consequently, liver and blood counts during these early time points depend upon injection technique rather than hepatic function. Based on standard assumptions (normality and negligible covariance) for error propagation (*27*), and the fact that $\tilde{Y}_{2j}$ was formed via multiplication by the above parameters, the determination of $\sigma(\tilde{y}_{ij})$ was based on the quadratic addition of the relative errors. Thus, values for

$\sigma(\tilde{Y}_{2j})^2$ were obtained from the following equation:

$$\sigma(\tilde{y}_{ij})^2 = \{[\sigma(y_{ij})/y_{ij}]^2 + [\sigma(V_p)/V_p]^2 + [\sigma(\tilde{I}_{24})/\tilde{I}_{24}]^2 + [\sigma(y_{2,24})/y_{2,24}]^2\}\tilde{y}_{ij}^2. \quad (9)$$

Calculations of $\sigma(\tilde{y}_{1j})$ used the assumption that the value of 1 in Eq. (3b) was exact. Finally, the reduced chi-square, χ_r^2, was calculated using m-2 degrees of freedom,

$$\chi_r^2 = \frac{\chi^2}{m-2}, \quad (10)$$

where m equaled the number of data points used to calculate χ^2 [Eq. (8)]. The probability, $P(\chi_r^2)$, of exceeding a given value of χ_r^2 was computed from the incomplete gamma function (*28*). A value <0.01 was considered a positive test of independence between data sets $\tilde{Y}$ and $\tilde{Y}'$.

RESULTS

Kinetic Data

Table 2 lists the pertinent physiochemical measurements acquired during each [Tc]NGA study. These parameters include: the galactose density and molar dose of the [Tc]NGA injection, liver weight, liver plasma flow measured by continuous infusion of ICG, hematocrit, plasma volume, and hepatic plasma volume. Table 3 lists the activity of each [Tc]NGA dose; the collimator (parallel hole) used during each study; the fraction of injected activity per liter of plasma, $\tilde{I}_{24}$, at 3 min (frame 24) postinjection; t_{70}, the time to reach 70% of the injected dose; the peak counts of each liver time-activity curve; percentage of the injected activity within the liver at the peak; and the time at which the peak occurred. Typical relative errors for the liver plasma flow measurements were 10%. Based on linear extrapolation of logarithmically transformed [^{125}I]HSA data, the typical relative error of the y-intercepts, and hence, the plasma volume calculations and t_{70} values, were ±5%. Plasma samples, when scaled to fraction of injected dose, accurately followed $\tilde{Y}_2$ up to 20 min postinjection, after which time they diverged by 5–20% below the ROI data.

Sensitivity Analysis

Table 4 lists the three variables that, according to our kinetic model, controlled the shape of the liver and blood time-activity curves. These variables were galactose density (ρ_{gal}), scaled hepatic plasma flow ($\tilde{F}$), and scaled molar dose ($\tilde{L}_o$).

The 12 studies produced 66 potential comparisons. Group I, which constituted the study pairs testable for hypothesis I, was comprised of five pairs. All pairs were consistent with the model ($C_1 = -1$) and tested positive ($P(\chi_r^2) < 0.01$) for independence. Group II, which constituted the study pairs testable for hypothesis II, contained four pairs. All pairs within Group II were consistent ($C_2 = -1$) and tested positive for independence. Group III contained 11 pairs. All pairs within this group were consistent ($C_3 = 1$) and independent ($P(\chi_r^2) < 0.003$). These pairs are listed in Table 5 with $\Delta\tilde{v}_k$, Δt_{70}, and χ_r^2. As listed in Table 6, all testable study pairs within each group were consistent and independent. We therefore rejected each null hypothesis (I, II, and III) and concluded that [Tc]NGA liver and plasma time-activity data is sensitive to scaled hepatic plasma flow, [Tc]NGA affinity, and receptor concentration.

Semiquantitative Analysis

Based on our index, $\Sigma\Delta\tilde{v}$, three of the 66 study pairs were inconsistent with the kinetic model: study pair 4 and 5, study pair 3 and 4, and study pair 1 and 4. The two latter study pairs have a positive change in t_{70} values with a negative $\Sigma\Delta\tilde{v}$, and thus reside in the lower right quadrant of Figure 4. Because the model predicts that a net increase (which is equivalent to a positive $\Sigma\Delta\tilde{v}$) in the sum of $\tilde{F}$, k_b, and [R] will result in a positive change in t_{70}, the semi-quantitative results of study pairs 3 and 4, and 1 and 4 are inconsistent with the kinetic model.

TABLE 3
Kinetic Data

Study no.	Dose (mCi)	Collimator	$\tilde{I}_{24}$ (l^{-1})	t_{70} (min)	Liver ROI at Peak: Counts (kcts)	%ID (%)	Time (min)
1	3.1	Hi sens	0.32	4.5	86	91	21.5
2	3.0	Hi sens	0.52	5.3	102	94	21.0
3	2.8	Hi sens	0.36	4.5	72	80	9.0
4	4.1	Hi sens	0.64	5.3	99	94	13.8
5	5.2	Hi res	0.51	4.5	40	83	>30.0
6	2.0	Hi sens	0.32	2.8	39	87	19.0
7	2.8	Hi sens	0.08	0.9	36	85	8.1
8	2.0	Hi sens	0.32	3.8	39	91	17.1
9	2.4	Hi sens	0.46	3.3	77	85	16.6
10	2.6	Hi sens	0.57	5.3	63	86	21.0
11	1.8	Hi sens	0.49	4.5	39	90	19.4
12	4.3	Hi sens	0.32	4.5	32	89	14.9

TABLE 4
Independent Variables

Study no.	Variables: Scaled* plasma flow (min^{-1})	Galactose† density (mole/mole)	Scaled‡ molar dose (μM/kg)
1	0.52	27	0.19
2	0.37	27	0.24
3	0.47	37	0.28
4	0.73	27	0.25
5	0.54	37	0.39
6	0.31	37	0.017
7	0.58	37	0.012
8	0.32	37	0.028
9	0.99	27	0.040
10	0.45	27	0.27
11	0.32	27	0.036
12	0.68	27	0.17

* Hepatic plasma flow per liter of plasma.
† mole of galactose per mole of HSA.
‡ mole of injected NGA per liter of plasma per kilogram of liver weight.

TABLE 5
Testable Study Pairs

Group*	Variable	Studies: $\tilde{Y}$	Studies: $\tilde{Y}'$	Model consistency: $\Delta\tilde{v}_k$	Model consistency: Δt_{70} (min)	$\chi^{2\dagger}_{\nu}$
I	$\tilde{F}$	1	2	−0.29	1.0	73.0
I	$\tilde{F}$	2	4	1.0	−0.2	6.2
I	$\tilde{F}$	2	10	0.064	−0.2	62.0
I	$\tilde{F}$	4	10	0.19	0.0	75.0
I	$\tilde{F}$	9	11	−0.67	1.2	81.0
II	ρ_{gal}	1	5	0.37	0.0	70.0
II	ρ_{gal}	3	4	−0.27	0.8	11.0
II	ρ_{gal}	3	10	−0.27	0.8	62.0
II	ρ_{gal}	8	10	−0.27	1.5	96.0
III	$\tilde{L}_o$	1	4	0.32	0.8	8.0
III	$\tilde{L}_o$	1	11	−0.81	0.0	19.0
III	$\tilde{L}_o$	2	11	−0.85	−1.0	95.0
III	$\tilde{L}_o$	3	5	0.39	0.0	29.0
III	$\tilde{L}_o$	3	6	−0.94	−1.8	42.0
III	$\tilde{L}_o$	4	11	−0.86	−0.8	23.0
III	$\tilde{L}_o$	4	12	−0.32	−0.8	26.0
III	$\tilde{L}_o$	5	6	−0.96	−1.8	100.0
III	$\tilde{L}_o$	5	8	−0.93	−0.8	66.0
III	$\tilde{L}_o$	10	11	−0.87	−0.8	78.0
III	$\tilde{L}_o$	11	12	3.72	0.0	1.2‡

$\nu = 450$.
* Criteria in Appendix.
† $P(\chi^2_\nu > 6.0) < 0.001$.
‡ $P(\chi^2_\nu) = 0.003$.

Study Pair Examples

Figure 5 provides two examples of kinetic sensitivity to scaled liver plasma flow. Studies 1 and 2 (Fig. 5A) employed the same carbohydrate density (27 gal/HSA) and similar scaled molar dose (study 1: 1.9×10^{-7} M/kg, and study 2: 2.4×10^{-7} M/kg). The scaled liver plasma flows within this pair were different (study 1: 0.52 min^{-1}, and study 2: 0.37 min^{-1}). Hepatic uptake of [Tc]NGA during study 1 was more rapid than study 2. Chi-square analysis [Eq. (8)] of this data pair yielded a probability of < 0.001 (Table 5) that both data sets came from the same sample population. Studies 9 and 11 (Fig. 5B) also employed a [Tc]NGA preparation of 27 gal/HSA, and similar scaled molar doses (Study 9, 0.40×10^{-7} M/kg; Study 11, 0.36×10^{-7} M/kg). The hepatic uptake and plasma clearance of Study 9 was more rapid than Study 11. This was consistent with a higher scaled hepatic plasma flow, $\tilde{F} = 0.98$ min^{-1}, during Study 9. The scaled hepatic plasma flow during Study 11 was 0.32 min^{-1}.

Figure 6 provides an example of kinetic sensitivity to ligand-receptor affinity. Studies 3 and 4 used [Tc]NGA preparations of differing galactose densities and hence differing ligand–receptor affinity: study 3, 37 gal/HSA; and study 4, 27 gal/HSA. The scaled molar doses were similar in magnitude: study 3, 0.28×10^{-7} M/kg; study 4, 0.25×10^{-7} M/kg. The scaled liver plasma flow during study 4, 0.74 min^{-1}, was nearly twice that of study 3, 0.47 min^{-1}. Hepatic uptake of [Tc]NGA during study 3 was more rapid and peaked earlier than study 4 despite an elevated scaled hepatic plasma flow during the latter study. Consequently, the more rapid uptake during study 3 could not be attributed to hepatic blood flow. The reduced chi-square [Eq. (10)] calculated for this pair equaled 100 ($P(\chi^2_\nu) < 0.001$) (Table 5).

Figure 7 provides an example of kinetic sensitivity to receptor concentration. Both studies 5 and 6 were consistent with the kinetic model and displayed dose-dependent uptake that could not be attributed to differing hepatic plasma flows. The scaled molar doses for each study were different: study 5, 3.9×10^{-7} M/kg; study 6, 0.17×10^{-7} M/kg. The scaled liver plasma flow during each study also differed: study 5, 0.55 min^{-1}; study 6, 0.48 min^{-1}. Despite a higher scaled hepatic plasma flow during study 5 (0.55 min^{-1} versus 0.48 min^{-1}), hepatic uptake of study 5 was less rapid than study 6 and did not achieve a peak within the 30-min study (Table 3). Chi-square analysis revealed a statistically significant difference ($P(\chi^2_\nu) < 0.001$) between data sets.

DISCUSSION

Sensitivity analysis when applied to a chemical (*29*) or biologic (*30*) system, provides a powerful tool for the optimization of an experimental design. Although the method of analysis is highly dependent upon the specific system and its application, most techniques fall into two classes. The first class simulates the system by a

TABLE 6
Conclusions

Hypothesis	Controlling parameter	Variable	Testable study pairs	Consistent study pairs	$P(\chi^2_\nu)$ <0.01	Reject null hypothesis
I	$\tilde{Q}$	$\tilde{Q}$	5	5	5	Yes
II	k_b	ρ_{gel}	4	4	4	Yes
III	[R]	$\tilde{L}_o$	11	11	11	Yes

mathematic model, and thus can be performed preexperimentally. Alternatively, the second class of methods studies the actual system by experimentally manipulating and recording its input and output. The two approaches are not mutually exclusive and each requires a conceptual model of the kinetic system. Although a mathematic model is not required, the second class depends upon a conceptual understanding of the system so that adequate controls may be placed during the analysis. We believe that this report is the first time the latter approach has been fully exploited to validate a radiopharmaceutical and model.

The Conceptual Model

Our conceptual model of the [Tc]NGA system contains four parameters: F/V_e, F/V_h, k_b, and [R]. The following physiologic and biochemical considerations were used to derive the model. First, the mechanism for tissue binding of [Tc]NGA is well documented at the biochemical level (*31*) and is known to be receptor-mediated. Thus, the binding phase of the kinetic model (Fig. 1) is composed of a second-order chemical reaction,

$$[L] + [R] \underset{k_{-b}}{\overset{k_b}{\rightleftarrows}} [C], \qquad (I)$$

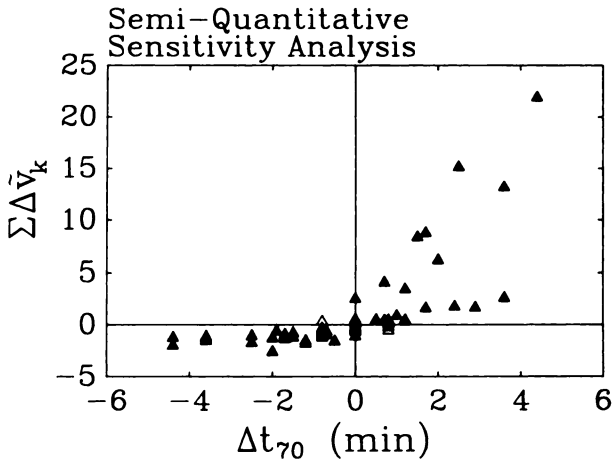

FIGURE 4
A semiquantitative analysis for kinetic sensitivity. Each point represents $\Sigma\Delta\tilde{v}$ and Δt_{70} values for a single study pair. According to this technique, the relative kinetic sensitivity of a study pair is inconsistent with the kinetic model if $\Sigma\Delta\tilde{v}$ and Δt_{70} lie in the lower right or upper left quadrants. Three study pairs were inconsistent (open triangles).

the rate of which can be expressed mathematically as

$$\frac{d[C]}{dt} = k_b[L][R] - k_{-b}[C], \qquad (II)$$

where [L] is the ligand concentration, NGA; [R] is the concentration of free receptor, HBP; [C] is the concentration of the resulting ligand-receptor complex; k_b is the forward-binding rate constant; and k_{-b} is the reverse-binding rate constant. Second, the reverse-binding rate constant of the NGA-HBP complex is extremely low and we have previously shown that it does not change with ligand carbohydrate density (*24*). Thus, dissociation of the ligand from the complex was set to zero by our model. Third, the receptor resides only in the liver; thus, the model required only liver and blood compartments. Fourth, the serum concentration of endogenous circulating ligand is extremely low (*32*), and can be ignored by the model. Fifth, [Tc]NGA is not pharmacologic; thus, experiments can be conducted which use differing amounts of injected ligand. Because ligand–receptor binding is a bimolecular reaction, increases in injected molar dose of ligand, L_o, would result in a higher percentage of occupied receptor. Sixth, the capillary lining of the liver permits free access of proteins (*33*), such as albumin, to the receptor which resides on the cell surface. As a result, a model of the NGA-HBP system did not require an interstitial space or an endothelial barrier. Consequently, only one process, the flow of plasma (F) through the liver, was required for the model to describe the delivery of ligand to the receptor. Thus, our model (*13*) used a scaled inflow, F/V_e, and a scaled outflow F/V_h. Seventh, excretion from the liver of Tc-labeled metabolites is negligible during the first 20 min of a [Tc]NGA study (*7, 23*). Lastly, organic anions (*34*), such as bilirubin or indocyanine green, do not bind to HBP. This fact permitted us to independently measure liver plasma flow via ICG extraction without modification of the kinetic model. This also means that [Tc]NGA imaging can be performed in patients with high serum bilirubin levels.

Of the four model parameters, F/V_e, F/V_h, k_b, and [R], three were selected for in vivo sensitivity analysis. The first, F/V_e, represents hepatic perfusion and permitted us to test sensitivity to liver plasma flow. We did not test the sensitivity of F/V_h. With the exception of severe hepatic congestion, a condition denoted by high

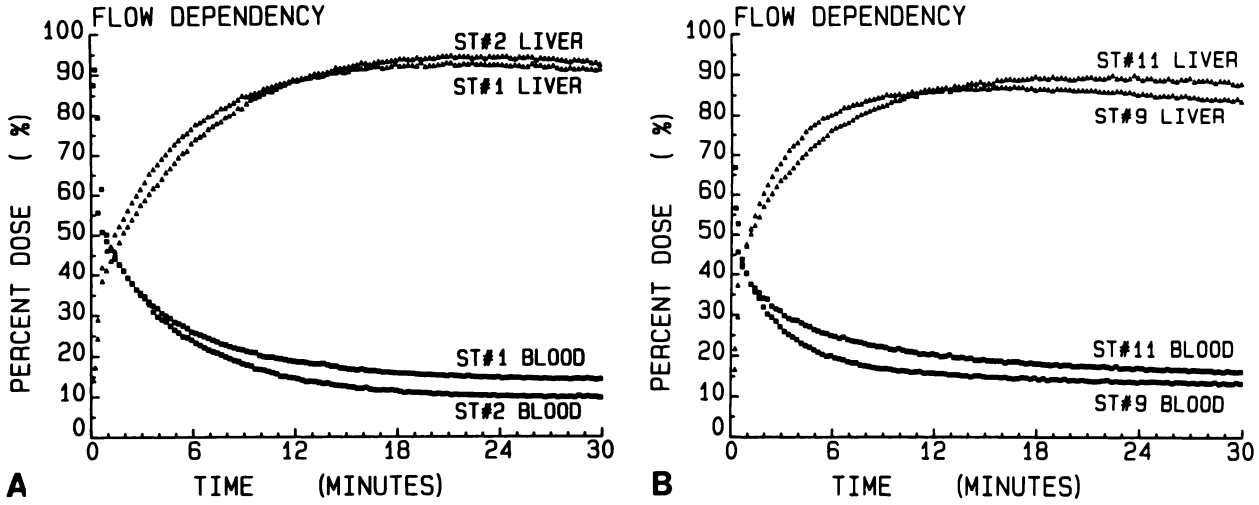

FIGURE 5

Flow-dependent uptake demonstrated kinetic sensitivity of [Tc]NGA time-activity data (only data from odd-valued frames are plotted) to alterations in hepatic plasma flow. A: Two pigs, studies 1 and 2, were injected with similar scaled molar doses and [Tc]NGA preparations of similar receptor affinity (Table 4). B: A second pair, studies 9 and 11, were studied at a lower scaled molar dose. Consistent with the kinetic model, the higher scaled hepatic plasma flow produced liver curves (triangles) with a faster rise and earlier peak.

arterial pressure, V_h is proportional to V_e within 5% (*35*). As a result, the ratio of parameter F/V_e to F/V_h would not differ during each study.

The second parameter included in our test was k_b. This parameter, when divided by the reverse-binding rate constant, forms the association constant, K_A, which is the standard equilibrium measure of ligand–receptor affinity. Because the reverse-binding rate constant is not altered by galactose density (*24*), the association constant is governed solely by variations in the forward-binding rate constant. Therefore, the observation of altered [Tc]NGA data as a result of changes in k_b was equivalent to a positive test of kinetic sensitivity by NGA-HBP affinity.

Receptor concentration was the third parameter

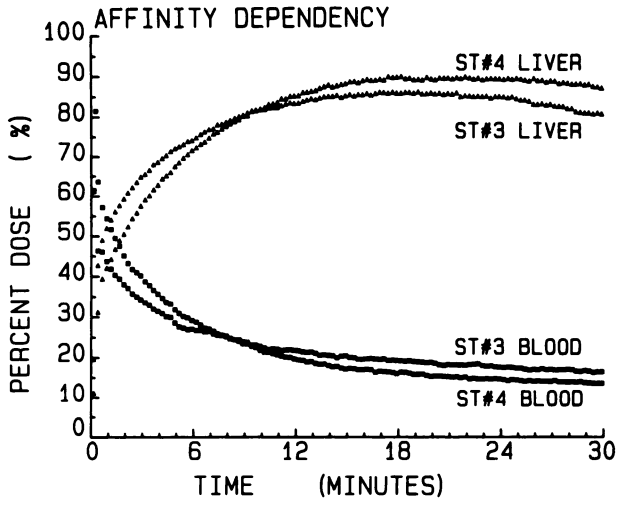

FIGURE 6

Affinity-dependent uptake demonstrated kinetic sensitivity of [Tc]NGA time-activity (only data-points from odd-valued frames are plotted) to alterations in ligand-receptor affinity. Two pigs were studied with similar scaled molar doses, but different galactose densities. The sharper initial rise exhibited by the liver curve of study 3 (triangle) could not be attributed to a higher scaled liver plasma flow.

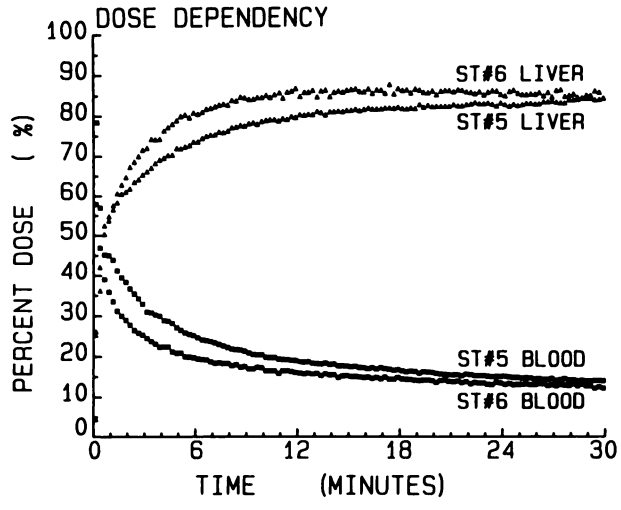

FIGURE 7

Dose dependent uptake demonstrated kinetic sensitivity of [Tc]NGA time-activity data (only data-points from odd-valued frames are plotted) to changes in receptor concentration. Two pigs, studies 5 and 6, were injected with NGAs of the same galactose density, but different scaled molar doses. The liver curve of study 6 had a sharper initial rise and peaked earlier even though the scaled plasma flow was lower.

tested for kinetic sensitivity. This test was based on the bimolecular nature of NGA-HBP binding; the rate of complex formation (Eq. II) is governed by both [L] and [R]. As a result, an assay for kinetic sensitivity to the concentration of receptor prior to the injection of [Tc] NGA is equivalent to a test for kinetic sensitivity to the initial concentration of the injected ligand. Thus, to carry out the sensitivity analysis of [R] we injected differing amounts of NGA. Analysis of these results required that we scale the amount in moles by plasma volume. The result was the initial in vivo concentration of NGA expressed in the amount of injected ligand per volume of plasma. Final scaling was achieved by normalizing this value to liver weight. This value in units of molar NGA per kilogram of liver is listed in Table 4 along with scaled plasma flow and galactose density, which together control hepatic uptake kinetics of [Tc] NGA.

Experimental Design

The ideal experimental design would consist of repetitive [Tc]NGA studies in three pairs of pigs. Each pair would be used to test a given parameter for kinetic sensitivity. Within each pair all of the physiologic variables except the tested parameter would be equal. One would then compare the liver and the blood time-activity data for changes in shape. For example, a test for kinetic sensitivity of the forward-binding rate constant would be conducted with [Tc]NGA injections of differing affinities into two animals having similar plasma volumes, hepatic plasma flows, and liver weights. The result would be two studies with differing ligand–receptor affinity, and the same scaled hepatic plasma flow and scaled molar dose. If the pharmacokinetic system was sensitive to [Tc]NGA affinity, each study would produce liver (and blood) time-activity curves with different shapes. Because the hepatic plasma flow of each pig could not be controlled, we studied 12 animals which yielded 66 study pairs. This gave us an adequate number of pairs testable for each parameter: five pairs for flow, four pairs for affinity, and 11 pairs for receptor concentration.

The goal of this experiment was to demonstrate in vivo kinetic sensitivity of [Tc]NGA to receptor concentration, ligand affinity, and hepatic plasma flow. The complexity of an in vivo analysis prevented us from controlling all of the variables within study pairs. As a result, it was not possible to isolate and quantify kinetic sensitivity of a given parameter or assign to each parameter an index of relative sensitivity, $\tilde{s}_{ik}$:

$$\tilde{s}_{ik} = \sum_{j}^{n} p'_k \Delta y_{ij} / \sigma(y_{ij})^2 \Delta p_k, \qquad (11)$$

where p'_k, the kth parameter of a specific member of a study pair, and $\sigma(y_{ij})^2$ serve as scale factors. Values for $\tilde{s}_{ik}$ would provide significant information regarding the optimal conditions of a given technique and could be used to select the best molar dose and NGA affinity for a patient with a given weight and state of health. Such information is more efficiently obtained through computer simulation and consequently, represents a second stage of our sensitivity analysis.

Because we could not calculate relative sensitivity exactly, we refer to the $\Sigma\Delta\tilde{v}$ index as semiquantitative. Although the plot of this index versus Δt_{70} permitted us to screen all study pairs for model consistency, it weighted the sensitivity of each parameter equally. As a result, even though inspection of pairs 3 and 4 (Fig. 6) confirmed sensitivity to ligand–receptor affinity, the semiquantitative technique [Eq. (6) and Fig. 4] overestimated the relative sensitivity of $\tilde{F}$ and calculated a negative $\Sigma\Delta\tilde{v}$. Examination of Table 5 reveals that, relative to ρ_{gal} (and hence k_b), large changes in $\tilde{F}$ were required to alter t_{70}. Thus, one would expect $\tilde{S}_{\tilde{F}}$, relative sensitivity to hepatic plasma flow, to be less than $\tilde{S}_{k_b}$. The three study pairs that failed the semiquantitative test utilized a high scaled molar dose of low affinity with a very high scaled plasma flow. Because time-activity curves are least sensitive to changes in $\tilde{F}$ under these conditions, a method that calculates net sensitivity with equal weighting for each parameter will overestimate the relative contribution of $\Delta\tilde{F}$ and the net result. Consequently, all pairs that include study 4 will be susceptible to this shortcoming of the semiquantitative method.

Significance

The most important goal during the design of a new radiopharmaceutical is delineation of the biological and chemical parameters that control image formation and time-activity data. Most investigations with new receptor-binding radiopharmaceuticals include a demonstration of in vivo displacement or blocking of the radiotracer by cold ligand. These experiments, which require large quantities of ligand, are not conducted under physiologic conditions, and consequently cannot establish the kinetic sensitivity of ligand affinity or receptor concentration when the tracer is used under clinical conditions. The [Tc]NGA affinities and scaled molar doses, as well as the observation scheme used in this study, were similar to our clinical protocol. As a result, this demonstration of kinetic sensitivity applies to [Tc] NGA studies of human subjects.

Furthermore, this study demonstrates that three physiologic parameters control the formation of [Tc] NGA time-activity data, and consequently, the formation of [Tc]NGA parenchymal images. Although sensitivity to three parameters complicates the interpretation of a single image, it is our contention that kinetic sensitivity to multiple physiologic parameters will increase the diagnostic power of a properly designed radiopharmaceutical.

APPENDIX

Criteria for the testable groups were as follows.

Group I: Scaled liver plasma flow

i: $\Delta\tilde{v}_{\rho_{gal}} \leq 0.1$ and $\text{sign}(\Delta\tilde{v}_{\tilde{L}_o}) = \text{sign}(\Delta\tilde{v}_{\tilde{F}})$ and $C_{\tilde{F}} = -1$,

or *ii*: $\Delta\tilde{v}_{\tilde{L}_o} \leq 0.1$ and $\text{sign}(\Delta\tilde{v}_{\rho_{gal}}) \neq \text{sign}(\Delta\tilde{v}_{\tilde{F}})$ and $C_{\tilde{F}} = -1$ and $C_{\rho_{gal}} = 1$,

or *iii*: $\Delta\tilde{v}_{\tilde{L}_o} \leq 0.1$ and $\Delta\tilde{v}_{\rho_{gal}} \leq 0.1$.

Group II: Carbohydrate density

i: $\Delta\tilde{v}_{\tilde{F}} \leq 0.1$ and $\text{sign}(\Delta\tilde{v}_{\tilde{L}_o}) = \text{sign}(\Delta\tilde{v}_{\rho_{gal}})$ and $C_{\rho_{gal}} = -1$,

or *ii*: $\Delta\tilde{v}_{\tilde{L}_o} \leq 0.1$ and $\text{sign}(\Delta\tilde{v}_{\tilde{F}}) \neq \text{sign}(\Delta\tilde{v}_{\rho_{gal}})$ and $C_{\rho_{gal}} = -1$ and $C_{\tilde{F}} = 1$,

or *iii*: $\Delta\tilde{v}_{\tilde{L}_o} \leq 0.1$ and $\Delta\tilde{v}_{\tilde{F}} \leq 0.1$.

Group III: Scaled molar dose

i: $\Delta\tilde{v}_{\tilde{F}} \leq 0.1$ and $\text{sign}(\Delta\tilde{v}_{\rho_{gal}}) = \text{sign}(\Delta\tilde{v}_{\tilde{L}_o})$ and $C_{\tilde{L}_o} = 1$,

or *ii*: $\Delta\tilde{v}_{\rho_{gal}} \leq 0.1$ and $\text{sign}(\Delta\tilde{V}_{\tilde{F}}) = \text{sign}(\Delta\tilde{v}_{\tilde{L}_o})$ and $C_{\tilde{L}_o} = 1$,

or *iii*: $\Delta\tilde{v}_{\rho_{gal}} \leq 0.1$ and $\Delta\tilde{v}_{\tilde{F}}$.

ACKNOWLEDGMENTS

The authors thank Drs. Kenneth A. Krohn, Paul O. Scheibe, and William C. Eckelman for valuable discussions and critical reviews. They also acknowledge the excellent technical assistance of Dusan P. Hutak. This research was supported by Public Health Service Grants RO1-AM34768, RO1-AM34706, and T32-GM07860.

REFERENCES

1. Garnett ES, Firnau G, Nahmias C. Dopamine visualized in the basal ganglia of living man. *Nature* 1983; 305:137–138.
2. Wagner HN Jr, Burns HD, Dannals RF, et al. Imaging dopamine receptors in the human brain by positron tomography. *Science* 1983; 221:1264–1266.
3. Eckelman WC, Reba RC, Rzeszotarski WJ, et al. External imaging of cerebral muscarinic acetylcholine receptors. *Science* 1984; 223:291–293.
4. Arnett CD, Shiue C-Y, Wolf AP, et al. Comparision of three ^{18}F-labeled butyrophenone neuroleptic drugs in the baboon using positron emission tomography. *J Neurochem* 1985; 44:835–844.
5. Farde L, Ehrin E, Eriksson L, et al. Substituted benzamides as ligands for visualization of dopamine receptor binding in the human brain by positron emission tomography. *Proc Natl Acad Sci USA* 1985; 82:3863–3867.
6. Syrota A, Comar D, Paillotin G, et al. Muscarinic cholinergic receptor in the human heart evidenced under physiological conditions by positron emission tomography. *Proc Natl Acad Sci USA* 1985; 82:584–588.
7. Stadalnik RC, Vera DR, Woodle ES, et al. Technetium-99m NGA functional hepatic imaging: Preliminary clinical experience. *J Nucl Med* 1985; 26:1233–1242.
8. Kilbourn MR, Zalutsky MR. Research and clinical potential of receptor based radiopharmaceuticals. *J Nucl Med* 1985; 26:655–662.
9. Stadalnik RC, Vera DR, Krohn KA. Receptor-binding radiopharmaceuticals: Experimental and clinical aspects. In: Freeman LM, ed. *Nuclear Medicine Annual 1986*. New York: Raven Press, 1986: 105–139.
10. Andreasen NC. Brain imaging: Applications in psychiatry. *Science* 1988; 239:1381–1388.
11. Mintun MA, Raichle ME, Kilbourn MR, Wooten GF, Welch MJ. A quantitative model for the in vivo assessment of drug-binding sites with positron emission tomography. *Ann Neurol* 1984; 15:217–227.
12. Wong DF, Wagner HN Jr, Dannels RF, et al. Effects of age on dopamine and serotonin receptors measured by positron tomography in the living human brain. *Science* 1984; 226:1393–1396.
13. Vera DR, Krohn KA, Scheibe PO, Stadalnik RC. Identifiability analysis of an in vivo receptor-binding radiopharmacokinetic system. *IEEE Trans Biomed Eng* 1985; BME-32:311–322.
14. Wong DF, Gjedde A, Wagner HN Jr. Quantification of neuroreceptors in the living human brain. I. Irreversible binding of ligands. *J Cereb Blood Flow Metab* 1986; 6:147–153.
15. Wong DF, Gjedde A, Wagner HN Jr, et al. Quantification of neuroreceptors in the living human brain. II. Inhibition studies of receptor density and affinity. *J Cereb Blood Flow Metab* 1986; 6:147–153.
16. Perlmutter JS, Larson KB, Raichle ME, et al. Strategies for in vivo measurement of receptor binding using positron emission tomography. *J Cereb Blood Flow Metab* 1986; 6:154–169.
17. Farde L, Hall H, Ehrin E, Sedvall G. Quantitative analysis of D2 dopamine receptor binding in the living human brain by PET. *Science* 1986; 231:258–261.
18. Baron JC, Maziere B, Loc'h C et al. Progressive supranuclear palsy: Loss of striatal dopamine receptors demonstrated in vivo by positron tomography. *Lancet* 1985; *i*:1163–1164.
19. Holman BL, Gibson RE, Hill TC, Eckelman WC, Albert M, Reba RC. Muscarinic acetylcholine receptors in Alzheimer's disease. *JAMA* 1985; 254:3063–3066.
20. Calne DB, Langston JW, Martin WRW, et al. Positron emission tomography after MPTP: observations relating to the cause of Parkinson's disease. *Nature* 1985; 317:246–248.
21. Samson Y, Bernuau J, Pappata S, et al. Cerebral uptake of benzodiazepine measured by positron emission tomography in hepatic encephalopathy. *N Engl J Med* 1987; 316:414–415.
22. Caesar J, Shaldon S, Chiandussi L, et al. The use of indocyanine green in the measurement of hepatic blood flow and as a test of hepatic function. *Clin Sci* 1961; 21:43–57.
23. Vera DR, Stadalnik RC, Krohn KA. [Tc-99m]-galactosyl-neoglycoalbumin: preparation and preclinical studies. *J Nucl Med* 26: 1985;1157–1167.
24. Vera DR, Krohn KA, Stadalnik RC, Scheibe PO. Tc-99m galactosyl-neoglycoalbumin: in vitro characterization of receptor-mediated binding. *J Nucl Med* 1984; 25:779–787.
25. Woodle ES, Vera DR, Stadalnik RC, Ward RE. Tc-NGA imaging in liver transplantation: preclinical studies. *Surgery* 1987; 102:55–62.
26. Fick A. Über die messung des blutguantums in den

herzventrikeln. *Verhandl Phys Med Ges Wurzburg* 1870; 2:XVI.
27. Bevington PR. Data reduction and error analysis for the physical sciences. New York: McGraw Hill, 1969:66–89.
28. Press WH, Flannery BP, Teukolsky SA, Velterling VT. Numerical recipes. Cambridge: Cambridge University Press, 1986:160–165.
29. Edelson D. Computer simulation in chemical kinetics. *Science* 1981; 214:981–986.
30. Bogumil RJ. Sensitivity analysis of biosystem models. *Fed. Proc.* 1980; 39:97–103.
31. Stockert RJ, Morell AG. Hepatic binding protein: the galactose-specific receptor of mammalian hepatocytes. *Hepatology* 1983; 3:750–757.
32. Ashwell G, Steer CJ. Hepatic recognition and catabolism of serum glycoproteins. *JAMA* 1981; 246:2358–2364.
33. Goresky CA. A linear method for determining liver sinusoidal and extravascular volumes. *Am J Physiol* 1963; 204:626–640.
34. Stockert RJ, Gärtner U, Morell AG, et al. Effects of receptor-specific antibody on the uptake of desialylated glycoproteins in the isolated perfused rat liver. *J Biol Chem* 1980; 255:3830–3831.
35. Guyton AC. Textbook of medical physiology. 7th Edition. Chap. 29. Philadelphia: W.B. Saunders, 1986.